The Journal of Chemical Physics

Which form of the molecular Hamiltonian is the most suitable for simulating the nonadiabatic quantum dynamics at a conical intersection?

Cite as: J. Chem. Phys. **153**, 211101 (2020); https://doi.org/10.1063/5.0033410
Submitted: 15 October 2020 . Accepted: 13 November 2020 . Published Online: 02 December 2020

Seonghoon Choi, and Jiří Vaníček

The Journal of Chemical Physics COMMUNICATION scitation.org/journal/jcp

Which form of the molecular Hamiltonian is the most suitable for simulating the nonadiabatic quantum dynamics at a conical intersection?

Cite as: J. Chem. Phys. 153, 211101 (2020); doi: 10.1063/5.0033410
Submitted: 15 October 2020 • Accepted: 13 November 2020 •
Published Online: 2 December 2020

Seonghoon Choi[a] and Jiří Vaníček[b]

AFFILIATIONS

Laboratory of Theoretical Physical Chemistry, Institut des Sciences et Ingénierie Chimiques, Ecole Polytechnique Fédérale de Lausanne (EPFL), CH-1015 Lausanne, Switzerland

[a]Electronic mail: seonghoon.choi@epfl.ch
[b]Author to whom correspondence should be addressed: jiri.vanicek@epfl.ch

ABSTRACT

Choosing an appropriate representation of the molecular Hamiltonian is one of the challenges faced by simulations of the nonadiabatic quantum dynamics around a conical intersection. The adiabatic, exact quasidiabatic, and strictly diabatic representations are exact and unitary transforms of each other, whereas the approximate quasidiabatic Hamiltonian ignores the residual nonadiabatic couplings in the exact quasidiabatic Hamiltonian. A rigorous numerical comparison of the four different representations is difficult because of the exceptional nature of systems where the four representations can be defined exactly and the necessity of an exceedingly accurate numerical algorithm that avoids mixing numerical errors with errors due to the different forms of the Hamiltonian. Using the quadratic Jahn–Teller model and high-order geometric integrators, we are able to perform this comparison and find that only the rarely employed exact quasidiabatic Hamiltonian yields nearly identical results to the benchmark results of the strictly diabatic Hamiltonian, which is not available in general. In this Jahn–Teller model and with the same Fourier grid, the commonly employed approximate quasidiabatic Hamiltonian led to inaccurate wavepacket dynamics, while the Hamiltonian in the adiabatic basis was the least accurate, due to the singular nonadiabatic couplings at the conical intersection.

I. INTRODUCTION

Many physical and chemical phenomena proceed via conical intersections—nuclear geometries where adiabatic potential energy surfaces of two or more electronic states intersect.[1–5] The conical intersections, which are much more ubiquitous[6–9] than previously believed, are responsible for the failure of the celebrated Born–Oppenheimer approximation that treats the electronic and nuclear motions in molecules separately. To correctly describe processes involving conical intersections, methods going beyond[10–18] the Born–Oppenheimer approximation must be used. Often, it is necessary to take into account multiple strongly coupled electronic states,[10,19,20] and in the adiabatic basis, one must consider the geometric phase effect—the sign change in adiabatic electronic states along a closed path encircling a conical intersection.[21–32]

Simulating the nonadiabatic quantum dynamics at a conical intersection using the adiabatic Hamiltonian, obtained from the electronic structure calculations, is problematic due to both the geometric phase effect[21,24,27–32] and singular nonadiabatic couplings.[20] These are rectified by a unitary transformation into the equivalent exact quasidiabatic Hamiltonian. Unlike the adiabatic electronic states, which are only coupled through the nonadiabatic couplings, the quasidiabatic states have both the residual, presumably small, nonadiabatic couplings and the diabatic couplings—the off-diagonal

elements of the potential energy matrix. However, the exact quasidiabatic Hamiltonian is rarely used. Instead, the approximate quasidiabatic Hamiltonian, which ignores the residual nonadiabatic couplings, is almost always used due to its simplicity. The separable form of the approximate quasidiabatic Hamiltonian allows using a wider range of time propagation schemes,[33–36] including the well-known split-operator algorithm,[37–39] but ignoring the residual nonadiabatic couplings decreases the accuracy.[40] The strictly diabatic Hamiltonian, with only diabatic couplings and no nonadiabatic couplings, would be the most suitable for the nonadiabatic quantum dynamics simulation. However, in typical systems, the strictly diabatic states only exist, in general, when an infinite number of electronic states are considered.[41,42]

Advantages and disadvantages of various Hamiltonians have been explored by numerous comparisons of the nonadiabatic quantum dynamics simulated with different Hamiltonians: To name a few, there exist comparisons between the strictly diabatic and approximate quasidiabatic Hamiltonians,[42–46] between the adiabatic and approximate quasidiabatic Hamiltonians,[47–49] between the adiabatic and exact quasidiabatic Hamiltonians,[50,51] and between the adiabatic and strictly diabatic Hamiltonians.[31,52,53] To the best of our knowledge, no study has compared all four different Hamiltonians—the adiabatic, exact quasidiabatic, approximate quasidiabatic, and strictly diabatic Hamiltonians—on a single system. A rigorous comparison is challenging because one must have both an appropriate system, where the different Hamiltonians are defined exactly, and a highly accurate numerical integrator, which allows separating numerical errors from the errors due to using different forms of the Hamiltonian.

The two-dimensional, two-state quadratic $E \otimes e$ Jahn–Teller model[46,54,55] is perfect for this comparison because analytical expressions exist for potential energy surfaces and nonadiabatic couplings in both the adiabatic and quasidiabatic representations and because this model has—exceptionally—a strictly diabatic Hamiltonian.

As for numerical integrators, the split-operator algorithms[37–39] are applicable to both the approximate quasidiabatic and strictly diabatic Hamiltonians because these Hamiltonians are separable, i.e., they can be expressed as sums of terms depending purely on either the position or the momentum operator. In contrast, neither the adiabatic nor exact quasidiabatic Hamiltonian is separable due to the nonvanishing nonadiabatic couplings. Although the split-operator algorithms cannot be used, the wavepacket can be propagated with the implicit midpoint method.[36,56] Both the split-operator and implicit midpoint methods preserve most geometric properties of the exact solution (such as norm conservation, stability, and time reversibility) and, in addition, can be symmetrically composed[36,57–59] to obtain integrators of arbitrary even order in the time step.[60,61] By taking advantage of the suitable model and high-order geometric integrators, we numerically compared the wavepacket and observables obtained from simulations with the different Hamiltonians: the adiabatic, exact quasidiabatic, approximate quasidiabatic, and strictly diabatic Hamiltonians.

II. THEORY

The molecular Hamiltonian can be partitioned as $\mathcal{H} = \mathcal{T}_\mathrm{N} + \mathcal{H}_\mathrm{e}(Q)$, where $\mathcal{T}_\mathrm{N}$ is the nuclear kinetic energy operator and $\mathcal{H}_\mathrm{e}(Q)$ denotes the electronic Hamiltonian, which depends parametrically on the D-dimensional vector Q of nuclear coordinates. Using the adiabatic electronic states $|n(Q)\rangle$, obtained by solving the time-independent Schrödinger equation,

$$\mathcal{H}_\mathrm{e}(Q)|n(Q)\rangle = V_n(Q)|n(Q)\rangle, \tag{1}$$

one can establish an approximate ansatz

$$\begin{aligned}|\Psi(Q,t)\rangle &= \sum_{n=1}^{S} \psi_n(Q,t)|n(Q)\rangle \\ &= \sum_{n=1}^{S} [\psi_n(Q,t)e^{-iA_n(Q)}][e^{iA_n(Q)}|n(Q)\rangle]\end{aligned} \tag{2}$$

for the solution of the time-dependent Schrödinger equation,

$$i\hbar\frac{\partial}{\partial t}|\Psi(Q,t)\rangle = \mathcal{H}|\Psi(Q,t)\rangle. \tag{3}$$

In Eqs. (1) and (2), $\psi_n(Q, t)$, $V_n(Q)$, and $e^{iA_n(Q)}$ are the time-dependent nuclear wavefunction, potential energy surface, and coordinate-dependent phase factor associated with the nth adiabatic electronic state. The Born–Huang expansion[62] in Eq. (2) is not exact unless the sum includes an infinite number of terms but can be very accurate if a finite number S of electronic states are chosen wisely.[10,63,64]

One is free to choose an overall phase $A_n(Q)$ in Eq. (2) because if $|n(Q)\rangle$ is a normalized solution of Eq. (1), then so is $e^{iA_n(Q)}|n(Q)\rangle$. Unless $A_n(Q)$ is carefully chosen, however, the adiabatic states and, therefore, also the wavepackets undergo a sign change along a closed path encircling a conical intersection.[3,21–32] In Sec. S4 of the supplementary material, we show that neglecting this double-valuedness of the wavepackets is detrimental to accuracy. Instead, in what follows, we set phases $A_n(Q)$ appropriately (see Sec. S1 of the supplementary material) to ensure the single-valuedness of both the adiabatic states and the wavepackets. In other words, we include the "geometric phase" in the adiabatic states in order to obtain the best possible results in the adiabatic representation. From now on, we absorb the overall phase factors $e^{-iA_n(Q)}$ and $e^{iA_n(Q)}$ into the nuclear wavefunctions $\psi_n(Q, t)$ and adiabatic states $|n(Q)\rangle$.

The time-dependent Schrödinger equation in the adiabatic representation,

$$i\hbar\frac{d}{dt}\boldsymbol{\psi}(t) = \hat{\mathbf{H}}_\mathrm{ad}\boldsymbol{\psi}(t), \tag{4}$$

is obtained by substituting ansatz (2) into Eq. (3) and projecting onto electronic states $\langle m(Q)|$ for $m \in \{1, \ldots, S\}$. Note that we have introduced the representation-independent matrix notation: bold font indicates either an $S \times S$ matrix, i.e., an electronic operator, or an S-dimensional vector, and the hat ($\hat{}$) indicates a nuclear operator. In particular, $(\hat{\mathbf{H}}_\mathrm{ad})_{mn} = \langle m|\mathcal{H}|n\rangle$ is the adiabatic Hamiltonian, and $\boldsymbol{\psi}(t)$ denotes the molecular wavepacket in the adiabatic representation with components $\psi_n(t)$; henceforth, $m, n \in \{1, \ldots, S\}$ unless otherwise stated. The formal solution of Eq. (4) for a given initial condition $\boldsymbol{\psi}(0)$ is

$$\psi_{\mathrm{ad}}(t) := \hat{\mathbf{U}}_{\mathrm{ad}}(t)\psi(0), \tag{5}$$

where $\hat{\mathbf{U}}_{\mathrm{ad}}(t)$ denotes the exact evolution operator $\hat{\mathbf{U}}_i(t) := \exp(-i\hat{\mathbf{H}}_i t/\hbar)$, with $i = \mathrm{ad}$. The adiabatic Hamiltonian $\hat{\mathbf{H}}_{\mathrm{ad}}$ is often expressed as

$$\hat{\mathbf{H}}_{\mathrm{ad}} = \frac{1}{2M}[\hat{P}^2\mathbf{1} - 2i\hbar\mathbf{F}_{\mathrm{ad}}(\hat{Q})\cdot\hat{P} - \hbar^2\mathbf{G}_{\mathrm{ad}}(\hat{Q})] + \mathbf{V}_{\mathrm{ad}}(\hat{Q}), \tag{6}$$

where we have used the matrix notation for the diagonal adiabatic potential energy matrix $[\mathbf{V}_{\mathrm{ad}}(Q)]_{mn} := V_n(Q)\delta_{mn}$, nonadiabatic vector couplings $[\mathbf{F}_{\mathrm{ad}}(Q)]_{mn} := \langle m(Q)|\nabla n(Q)\rangle$, and nonadiabatic scalar couplings $[\mathbf{G}_{\mathrm{ad}}(Q)]_{mn} := \langle m(Q)|\nabla^2 n(Q)\rangle$. The D-dimensional vector P is the nuclear momentum conjugate to Q, and the dot $(\cdot)$ denotes a dot product in the D-dimensional nuclear vector space; we use the mass-scaled coordinates for simplicity.

Expressing the nonadiabatic vector couplings as

$$[\mathbf{F}_{\mathrm{ad}}(Q)]_{mn} = \frac{\langle m(Q)|\nabla\mathcal{H}_{\mathrm{e}}(Q)|n(Q)\rangle}{V_n(Q) - V_m(Q)}, \quad m \neq n, \tag{7}$$

shows that they are singular at a conical intersection,[65] which is a nuclear geometry Q_0, where $V_m(Q_0) = V_n(Q_0)$ for $m \neq n$.[11,20,66] This singularity causes problems for the nonadiabatic dynamics simulations especially for the grid-based methods because an infinitely dense grid would be required to describe the singularity. The singularity, however, can be removed by a coordinate-dependent unitary transformation of Hamiltonian (6) into its quasidiabatic representation,

$$\begin{aligned}\hat{\mathbf{H}}_{\text{qd-exact}} &= \mathbf{S}(\hat{Q})\hat{\mathbf{H}}_{\mathrm{ad}}\mathbf{S}(\hat{Q})^\dagger \\ &= \frac{1}{2M}[\hat{P}^2\mathbf{1} - 2i\hbar\mathbf{F}_{\mathrm{qd}}(\hat{Q})\cdot\hat{P} - \hbar^2\mathbf{G}_{\mathrm{qd}}(\hat{Q})] + \mathbf{V}_{\mathrm{qd}}(\hat{Q}),\end{aligned} \tag{8}$$

where $\mathbf{F}_{\mathrm{qd}}(Q)$ and $\mathbf{G}_{\mathrm{qd}}(Q)$ denote the residual nonadiabatic vector and scalar couplings, respectively. Different transformation matrices $\mathbf{S}(Q)$ are obtained by different quasidiabatization schemes,[65] which include the block-diagonalization of the reference Hamiltonian matrix,[44,67–69] integration of the nonadiabatic couplings,[70–74] use of the molecular properties,[75–81] and construction of regularized quasidiabatic states.[43,46,82] We have chosen the regularized diabatization scheme because it is simple to implement and because it removes the conical intersection singularity reliably and efficiently.[83] The choice of quasidiabatization affects the magnitude of the residual couplings and, therefore, their importance for the accuracy of nonadiabatic simulations.[40]

The initial state can be propagated with $\hat{\mathbf{H}}_{\text{qd-exact}}$ instead of $\hat{\mathbf{H}}_{\mathrm{ad}}$ to obtain the solution

$$\psi_{\text{qd-exact}}(t) := \mathbf{S}(\hat{Q})^\dagger\hat{\mathbf{U}}_{\text{qd-exact}}(t)\mathbf{S}(\hat{Q})\psi(0), \tag{9}$$

which is equivalent to $\psi_{\mathrm{ad}}(t)$. However, it is much more common to use the simpler approximate quasidiabatic Hamiltonian,

$$\hat{\mathbf{H}}_{\text{qd-approx}} = \frac{\hat{P}^2}{2M}\mathbf{1} + \mathbf{V}_{\mathrm{qd}}(\hat{Q}). \tag{10}$$

This approximation is typically justified only heuristically by referring to the "small" magnitude of the residual nonadiabatic couplings. Nevertheless, the solution

$$\begin{aligned}\psi_{\text{qd-approx}}(t) &:= \mathbf{S}(\hat{Q})^\dagger\hat{\mathbf{U}}_{\text{qd-approx}}(t)\mathbf{S}(\hat{Q})\psi(0) \\ &\approx \psi_{\text{qd-exact}}(t)\end{aligned} \tag{11}$$

obtained using $\hat{\mathbf{H}}_{\text{qd-approx}}$ is not exact and would still be only approximate even if evaluated numerically exactly.

We have numerically compared the three different solutions, $\psi_{\mathrm{ad}}(t)$, $\psi_{\text{qd-exact}}(t)$, and $\psi_{\text{qd-approx}}(t)$ using the archetypal quadratic $E\otimes e$ Jahn–Teller model.[46,54] In the model, two electronic states labeled $n = 1$ and $n = 2$ are coupled by doubly degenerate normal modes Q_1 and Q_2. We express the potential energy surface in polar coordinates—the radius $\rho(Q) := \sqrt{Q_1^2 + Q_2^2}$ and polar angle $\phi(Q) := \arctan(Q_2/Q_1)$ in the space of the degenerate normal modes.[46,54] In addition, we work in natural units (n.u.) by setting $k = M = \hbar = 1$ n.u., where M is the mass associated with the degenerate normal modes and $\hbar\omega = \hbar\sqrt{k/M} = 1$ n.u. is the quantum of the vibrational energy of these modes.[54,55]

The adiabatic potential energy surfaces are $V_1(Q) = V_+(Q)$ and $V_2(Q) = V_-(Q)$, where $V_\pm(Q) := E_0(Q) \pm E_{\mathrm{cpl}}(Q)$ depends on the harmonic potential energy $E_0(Q) := k\rho(Q)^2/2$ and Jahn–Teller coupling[46,54]

$$E_{\mathrm{cpl}}(Q) := \rho(Q)[c_1^2 + 2c_1c_2\rho(Q)\cos 3\phi(Q) + c_2^2\rho(Q)^2]^{1/2}. \tag{12}$$

The nonadiabatic vector coupling is[46,54]

$$\mathbf{F}_{\mathrm{ad}}(Q) = -i\begin{pmatrix}\nabla\alpha(Q) & e^{2i\alpha(Q)}\nabla\theta(Q)\\ e^{-2i\alpha(Q)}\nabla\theta(Q) & -\nabla\alpha(Q)\end{pmatrix}, \tag{13}$$

with $\alpha(Q) := \phi(Q)/2$ and

$$\theta(Q) := \frac{1}{2}\arctan\frac{c_1\rho(Q)\sin\phi(Q) - c_2\rho(Q)^2\sin 2\phi(Q)}{c_1\rho(Q)\cos\phi(Q) + c_2\rho(Q)^2\cos 2\phi(Q)}. \tag{14}$$

In our study, the coupling coefficients were $c_1 = 1$ n.u. and $c_2 = 0.25$ n.u. Unlike the potential energy $\mathbf{V}_{\mathrm{ad}}(Q)$, the nonadiabatic couplings $\mathbf{F}_{\mathrm{ad}}(Q)$ and $\mathbf{G}_{\mathrm{ad}}(Q)$ are affected by overall phases of the adiabatic states. One of the most standard choices[46,54] of $A_n(Q)$ results in zero diagonal elements of $\mathbf{F}_{\mathrm{ad}}(Q)$ and double-valued adiabatic states (see Sec. S1 of the supplementary material); instead, we have chosen the phases $A_n(Q)$ so that the adiabatic states are single-valued and $\mathbf{F}_{\mathrm{ad}}(Q)$ contains nonzero diagonal elements [see Eq. (13)]. The relationship

$$\mathbf{G}_{\mathrm{ad}}(Q) = \nabla\cdot\mathbf{F}_{\mathrm{ad}}(Q) + \mathbf{F}_{\mathrm{ad}}(Q)^2 \tag{15}$$

holds exceptionally in the Jahn–Teller model and other systems in which a finite number of states represent the system exactly in both the adiabatic and diabatic representations. Relationship (15) allows us to re-express Hamiltonian (6) in a simpler form,

$$\hat{\mathbf{H}}_{\mathrm{ad}} = \frac{1}{2M}[\hat{P}\mathbf{1} - i\hbar\mathbf{F}_{\mathrm{ad}}(\hat{Q})]^2 + \mathbf{V}_{\mathrm{ad}}(\hat{Q}), \tag{16}$$

which would generally only hold for $S \to \infty$.

The exact quasidiabatic Hamiltonian

$$\begin{aligned}\hat{\mathbf{H}}_{\mathrm{qd\text{-}exact}} &= \mathbf{S}(\hat{Q})\hat{\mathbf{H}}_{\mathrm{ad}}\mathbf{S}(\hat{Q})^\dagger \\ &= \frac{1}{2M}[\hat{P}\mathbf{1} - i\hbar\mathbf{F}_{\mathrm{qd}}(\hat{Q})]^2 + \mathbf{V}_{\mathrm{qd}}(\hat{Q})\end{aligned} \tag{17}$$

is obtained from Hamiltonian (16) using the adiabatic to quasidiabatic transformation matrix,[43,46,82]

$$\mathbf{S}(Q) = \frac{1}{\sqrt{2}}\begin{pmatrix} e^{-2i\alpha(Q)} & 1 \\ 1 & -e^{2i\alpha(Q)} \end{pmatrix}. \tag{18}$$

In Eq. (17), the (no longer diagonal) quasidiabatic potential energy matrix is

$$\begin{aligned}\mathbf{V}_{\mathrm{qd}}(Q) &= \mathbf{S}(Q)\mathbf{V}_{\mathrm{ad}}(Q)\mathbf{S}(Q)^\dagger \\ &= \begin{pmatrix} E_0(Q) & E_{\mathrm{cpl}}(Q)e^{-2i\alpha(Q)} \\ E_{\mathrm{cpl}}(Q)e^{2i\alpha(Q)} & E_0(Q) \end{pmatrix},\end{aligned} \tag{19}$$

and the residual nonadiabatic coupling is[42]

$$\begin{aligned}\mathbf{F}_{\mathrm{qd}}(Q) &= \mathbf{S}(Q)\mathbf{F}_{\mathrm{ad}}(Q)\mathbf{S}(Q)^\dagger + \mathbf{S}(Q)\nabla\mathbf{S}(Q)^\dagger \\ &= -i\nabla\theta_-(Q)\begin{pmatrix} 1 & 0 \\ 0 & -1 \end{pmatrix},\end{aligned} \tag{20}$$

where $\theta_\pm(Q) := \theta(Q) \pm \alpha(Q)$ [$\theta_+(Q)$ will be used below].

In realistic systems, Eqs. (15) and (16) would only hold if an infinite number of electronic states were considered. Likewise, the strictly diabatic Hamiltonian does not, in general, exist unless $S \to \infty$.[41,42] Yet, due to its exceptional form, the Jahn–Teller Hamiltonian can be strictly diabatized[46] into a separable Hamiltonian

$$\hat{\mathbf{H}}_{\mathrm{diab}} = \frac{\hat{P}^2}{2M}\mathbf{1} + \mathbf{V}_{\mathrm{diab}}(\hat{Q}), \tag{21}$$

obtained by replacing the transformation matrix $\mathbf{S}(Q)$ in Eq. (18) with

$$\mathbf{T}(Q) = \frac{1}{\sqrt{2}}\begin{pmatrix} e^{-i\theta_+(Q)} & e^{-i\theta_-(Q)} \\ e^{i\theta_-(Q)} & -e^{i\theta_+(Q)} \end{pmatrix}. \tag{22}$$

The diabatic potential energy matrix is

$$\mathbf{V}_{\mathrm{diab}}(Q) = \mathbf{T}(Q)\mathbf{V}_{\mathrm{ad}}(Q)\mathbf{T}(Q)^\dagger = \begin{pmatrix} E_0(Q) & E_{\mathrm{cpl}}(Q)e^{-2i\theta(Q)} \\ E_{\mathrm{cpl}}(Q)e^{2i\theta(Q)} & E_0(Q) \end{pmatrix}. \tag{23}$$

Potential energy surfaces $\mathbf{V}_{\mathrm{ad}}(Q)$, $\mathbf{V}_{\mathrm{qd}}(Q)$, and $\mathbf{V}_{\mathrm{diab}}(Q)$ in the vicinity of the conical intersection $Q = 0$ are visualized in Fig. 1. The strictly diabatic states are only coupled by the off-diagonal elements in $\mathbf{V}_{\mathrm{diab}}(Q)$ because the residual nonadiabatic couplings vanish:

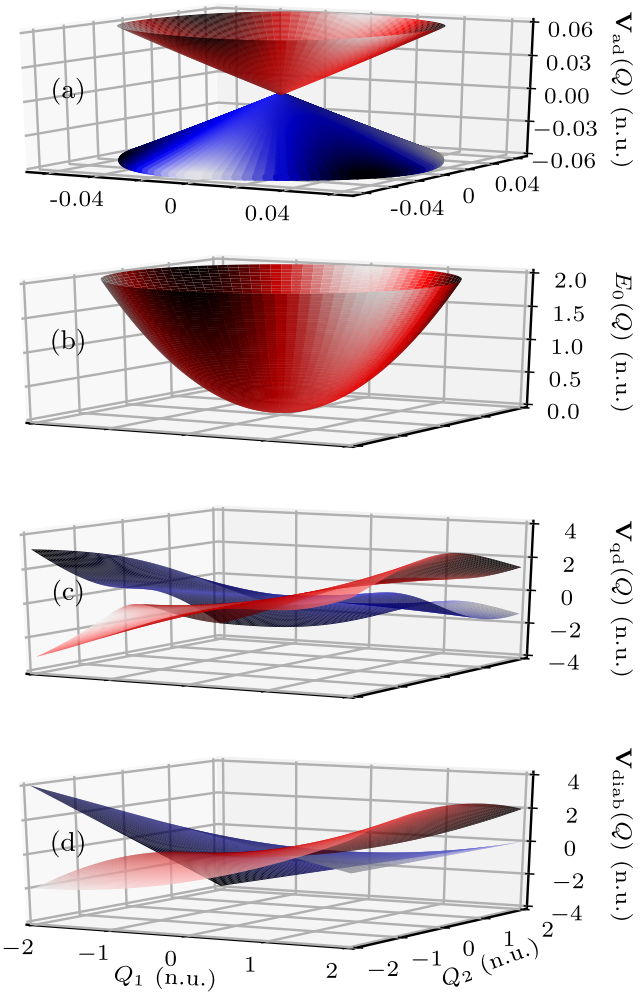

FIG. 1. Potential energy surfaces in the $E \otimes e$ Jahn–Teller model around the conical intersection $Q = 0$. (a) Adiabatic potential energy surfaces $V_1(Q) = V_+(Q)$ (red) and $V_2(Q) = V_-(Q)$ (blue); the two elements of the diagonal matrix $\mathbf{V}_{\mathrm{ad}}(Q)$ touch each other at the conical intersection. (b) Diagonal elements $[\mathbf{V}_{\mathrm{qd}}(Q)]_{11} = [\mathbf{V}_{\mathrm{qd}}(Q)]_{22} = [\mathbf{V}_{\mathrm{diab}}(Q)]_{11} = [\mathbf{V}_{\mathrm{diab}}(Q)]_{22} = E_0(Q)$ of the quasidiabatic and strictly diabatic potential energy matrices are shown together because they are all equal. Off-diagonal couplings of (c) the quasidiabatic $[\mathbf{V}_{\mathrm{qd}}(Q)]$ and (d) strictly diabatic $[\mathbf{V}_{\mathrm{diab}}(Q)]$ potential energy matrix; the real part $\mathrm{Re}[\mathbf{V}_i(Q)]_{12} = \mathrm{Re}[\mathbf{V}_i(Q)]_{21}$ is in red, and the imaginary part $\mathrm{Im}[\mathbf{V}_i(Q)]_{12} = -\mathrm{Im}[\mathbf{V}_i(Q)]_{21}$ is in blue for $i \in$ {qd, diab}.

$$\mathbf{F}_{\mathrm{diab}}(Q) = \mathbf{T}(Q)\mathbf{F}_{\mathrm{ad}}(Q)\mathbf{T}(Q)^\dagger + \mathbf{T}(Q)\nabla\mathbf{T}(Q)^\dagger = 0. \tag{24}$$

Like $\mathbf{F}_{\mathrm{ad}}(Q)$ and $\mathbf{G}_{\mathrm{ad}}(Q)$, the transformation matrices $\mathbf{S}(Q)$ and $\mathbf{T}(Q)$ in Eqs. (18) and (22) change according to overall phases of the adiabatic states (see Sec. S1 of the supplementary material).

We simulated the quantum dynamics following a transition from the ground vibrational eigenstate of the electronic state of A symmetry, $V_A(Q) = -E_{\mathrm{gap}} + E_0(Q)$, to the doubly degenerate states of the Jahn–Teller model by choosing the initial state as[46]

$$\tilde{\psi}(0) = \frac{e^{-\rho(Q)^2/2\hbar}}{\sqrt{2\pi\hbar}}\begin{pmatrix}1\\1\end{pmatrix}, \tag{25}$$

where $\tilde{\psi}(t) = \mathbf{T}(\hat{Q})\psi(t)$ denotes the wavepacket in the strictly diabatic representation. To obtain the initial wavepacket, we assumed an impulsive excitation, i.e., the validity of the time-dependent perturbation theory and Condon approximation during the excitation.

Among various time propagation schemes,[33–36] we chose the geometric integrators[36,38,56] because they preserve exactly geometric properties of the exact evolution. Second-order split-operator algorithms,[37–39] including the TVT algorithm (see Ref. 61 for our nomenclature of the split-operator algorithms), preserve the linearity, norm, inner-product, symplecticity, stability, symmetry, and time reversibility of the exact solution.[36,38,56] The implicit midpoint method, as well as the closely related trapezoidal rule (or Crank–Nicolson) method–[84,85] conserves, in addition, the energy. Both the split-operator and implicit midpoint methods can be symmetrically composed using various recursive or direct schemes[36,57–59] to obtain integrators of arbitrary even orders of accuracy;[60,61] these compositions conserve all the geometric properties that are conserved by the elementary methods (see Refs. 60 and 61 and Sec. S2 of the supplementary material). The composed[36,57,58] TVT split-operator algorithm was used to propagate the wavepacket with the separable Hamiltonians ($\hat{\mathbf{H}}_{\text{diab}}$ and $\hat{\mathbf{H}}_{\text{qd-approx}}$), whereas the composed implicit midpoint method[36,56] was employed for propagations with the nonseparable Hamiltonians ($\hat{\mathbf{H}}_{\text{ad}}$ and $\hat{\mathbf{H}}_{\text{qd-exact}}$). Both integrators were composed using the optimal[59] eighth-order scheme, which, when combined with a small time step of $\Delta t = 1/(40\omega) = 0.025$ n.u., led to time discretization errors negligible to the errors due to the use of different forms of the Hamiltonian (see Sec. S3 of the supplementary material).

On a grid of infinite range and density, nonadiabatic quantum dynamics simulated using $\hat{\mathbf{H}}_{\text{diab}}$, $\hat{\mathbf{H}}_{\text{ad}}$, and $\hat{\mathbf{H}}_{\text{qd-exact}}$ would be identical. Therefore, the comparison of these Hamiltonians is only meaningful for a specific finite grid; we used a uniform grid of 64 × 64 points defined between $Q_l = -10$ n.u. and $Q_l = 10$ n.u. for $l \in \{1, 2\}$. In addition, the favorable form of the strictly diabatic Hamiltonian allowed us to obtain the exact reference solution $\tilde{\psi}_{\text{ref}}(t) := \hat{\mathbf{U}}_{\text{diab}}(t)\tilde{\psi}(0)$ that is fully converged in both space and time: to ensure the grid convergence of the reference wavepacket, we used a grid of 128 × 128 points defined between $Q_l = -10\sqrt{2}$ n.u. and $Q_l = 10\sqrt{2}$ n.u. for $l \in \{1, 2\}$. In Sec. S3 of the supplementary material, we show that both the spatial and time discretization errors of $\tilde{\psi}_{\text{ref}}(t)$ are negligible ($<10^{-10}$). In contrast, even on an infinite grid, the wavepacket $\tilde{\psi}_{\text{qd-approx}}(t)$ would still not be exact because the residual nonadiabatic couplings are ignored. Section S3 of the supplementary material shows that even on a grid of 64 × 64 points, the spatial discretization errors are only minor contributors to the total errors of $\tilde{\psi}_{\text{qd-approx}}(t)$.

III. RESULTS AND DISCUSSION

We compared the nonadiabatic quantum dynamics simulated using the adiabatic ($\hat{\mathbf{H}}_{\text{ad}}$), exact quasidiabatic ($\hat{\mathbf{H}}_{\text{qd-exact}}$), and approximate quasidiabatic ($\hat{\mathbf{H}}_{\text{qd-approx}}$) Hamiltonians (see Sec. S4 of the supplementary material for the results obtained in the adiabatic representation without including the geometric phase). The reference quantum dynamics simulated using the strictly diabatic Hamiltonian $\hat{\mathbf{H}}_{\text{diab}}$ was left out of the comparison and was only used as the benchmark because $\hat{\mathbf{H}}_{\text{diab}}$ only exists, in general, when $S \to \infty$. Before comparing the wavepackets themselves, we first present a comparison of three computed observables: the power spectrum obtained by Fourier transforming the autocorrelation function $\langle\tilde{\psi}(0)|\tilde{\psi}(t)\rangle$ (Fig. 2), population $\mathcal{P}_1(t)$ of the first ($n = 1$) adiabatic electronic state (Fig. 3), and position $\langle\rho(t)\rangle$ (Fig. 4). The validity of this comparison is justified because the time discretization errors of the presented observables and the time and spatial discretization errors of the reference observables are negligible (see Sec. S3 of the supplementary material).

Panels (a) of Figs. 2–4 show that none of these observables is obtained accurately with the adiabatic Hamiltonian $\hat{\mathbf{H}}_{\text{ad}}$ even if the geometric phase is included: The positions and intensities of the peaks in the power spectrum are inaccurate, while the population $\mathcal{P}_{1,\text{ad}}(t)$ and position $\langle\rho(t)\rangle_{\text{ad}}$ deviate very rapidly from their benchmark values. In contrast, all three presented observables are computed extremely accurately if the wavepacket is propagated with the exact quasidiabatic Hamiltonian [see panels (b) of Figs. 2–4]. There is no visible difference between the observables obtained using $\hat{\mathbf{H}}_{\text{qd-exact}}$ and the benchmark observables obtained using $\hat{\mathbf{H}}_{\text{diab}}$.

Figure 2(c) shows that the spectrum obtained by Fourier transforming $\langle\tilde{\psi}(0)|\tilde{\psi}_{\text{qd-approx}}(t)\rangle$ is very similar to the benchmark spectrum; the differences are only clearly visible in the zoomed-in version [see the inset of Fig. 2(c)]. For applications that do not require extremely precise peak positions and intensities, even the spectrum obtained using $\hat{\mathbf{H}}_{\text{qd-approx}}$ would suffice. In contrast, in panels (c) of Figs. 3 and 4, we see that both the population and the position

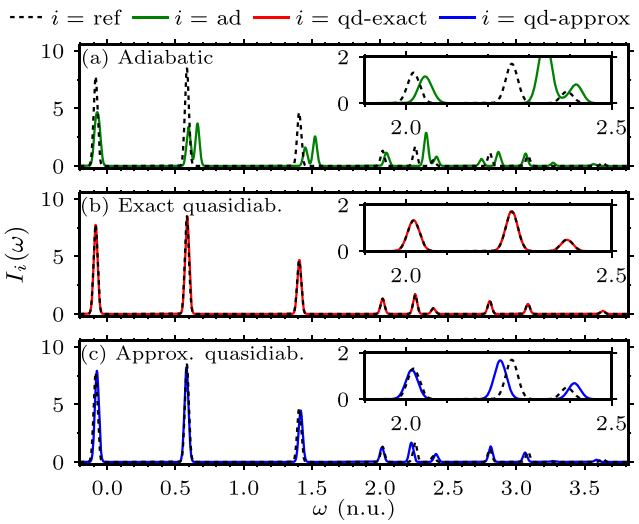

FIG. 2. Power spectrum computed by Fourier transforming the autocorrelation function $\langle\tilde{\psi}(0)|\tilde{\psi}_i(t)\rangle$ of the wavepacket propagated with the (a) adiabatic (i = ad), (b) exact quasidiabatic (i = qd-exact), or (c) approximate quasidiabatic (i = qd-approx) Hamiltonian is compared with the benchmark spectrum (i = ref). To emulate the broadening of the peaks, the autocorrelation function was multiplied by the damping function $f(t) = \exp[-(t/t_{\text{damp}})^2]$, with $t_{\text{damp}} = 80$ n.u., before the Fourier transformation. Zoomed-in versions of the spectra are presented in the insets.

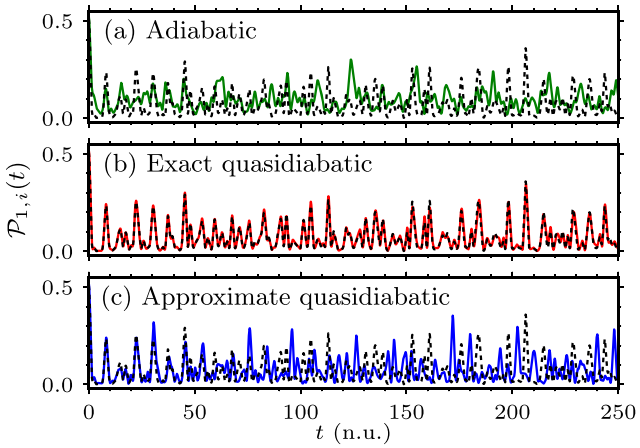

FIG. 3. Time dependence of the population $\mathcal{P}_{1,i}(t) := \langle\psi_i(t)|\mathbf{P}_1|\psi_i(t)\rangle$ of the first (n = 1) adiabatic electronic state obtained from the wavepacket propagated with the (a) adiabatic (i = ad), (b) exact quasidiabatic (i = qd-exact), or (c) approximate quasidiabatic (i = qd-approx) Hamiltonian is compared with the benchmark population $\mathcal{P}_{1,\mathrm{ref}}(t)$; $\mathbf{P}_n = |n\rangle\langle n|$ is the population operator of the nth state. The exact norm conservation by the employed geometric integrators (see Sec. S2 of the supplementary material) implies that the population of the second electronic state is $\mathcal{P}_{2,i}(t) = 1 - \mathcal{P}_{1,i}(t)$ for $i \in$ {ref, ad, qd-exact, qd-approx}. Line labels are the same as in Fig. 2.

obtained with the approximate quasidiabatic Hamiltonian become inaccurate already after $t \approx 50$ n.u. For $t > 50$ n.u., the population and position are described accurately only in simulations using either the exact quasidiabatic or strictly diabatic Hamiltonian. Among these Hamiltonians, however, only the exact quasidiabatic Hamiltonian exists, in general, unless $S \to \infty$.[41,42]

Some observables may be accurate, even if they are computed from a poor wavepacket. In contrast, an accurate wavepacket

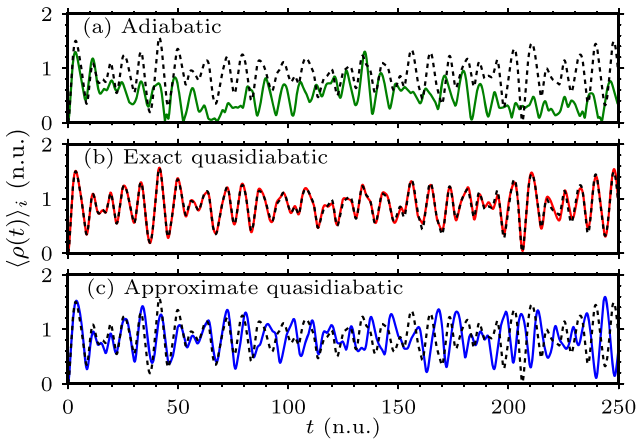

FIG. 4. Time dependence of the position $\langle\rho(t)\rangle_i := [\sum_{l=1}^{2}\langle\tilde{\psi}_i(t)|\hat{Q}_l|\tilde{\psi}_i(t)\rangle^2]^{1/2}$ obtained from the wavepacket propagated with the (a) adiabatic (i = ad), (b) exact quasidiabatic (i = qd-exact), or (c) approximate quasidiabatic (i = qd-approx) Hamiltonian is compared with the benchmark position $\langle\rho(t)\rangle_{\mathrm{ref}}$. Line labels are the same as in Fig. 2.

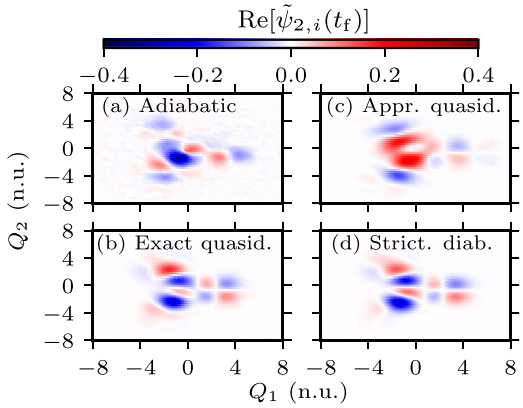

FIG. 5. Accuracy of the nonadiabatic quantum dynamics simulation demonstrated by comparing the wavepackets $\tilde{\psi}_i(t_f)$ at the final time of $t = t_f$ propagated with the (a) adiabatic (i = ad), (b) exact quasidiabatic (i = qd-exact), (c) approximate quasidiabatic (i = qd-approx), or (d) strictly diabatic (i = ref) Hamiltonian. The reference wavepacket $\tilde{\psi}_{\mathrm{ref}}(t)$ serves as the benchmark. We only show $\mathrm{Re}[\tilde{\psi}_{2,i}(t_f)]$, i.e., the real part of the nuclear wavepacket in the second (n = 2) electronic state of the strictly diabatic representation.

ensures the accuracy of every observable computed from it. For a more stringent comparison between the different Hamiltonians, in Fig. 5, we, therefore, display the wavepackets $\tilde{\psi}(t_f)$ at the final time. Whereas $\tilde{\psi}_{\text{qd-exact}}(t)$ resembles the exact wavepacket $\tilde{\psi}_{\mathrm{ref}}(t)$ closely and $\tilde{\psi}_{\text{qd-approx}}(t)$ has a similar overall shape but differs in the nodal structure and other details, $\tilde{\psi}_{\mathrm{ad}}(t)$ is completely different.

For a more quantitative comparison, we measure the error of the wavepacket $\tilde{\psi}(t)$ using quantum fidelity[86] $\mathcal{F}(t) := |\langle\tilde{\psi}_{\mathrm{ref}}(t)|\tilde{\psi}(t)\rangle|^2$ and distance $\mathcal{D}(t) := \|\tilde{\psi}(t) - \tilde{\psi}_{\mathrm{ref}}(t)\|$ between $\tilde{\psi}(t)$ and $\tilde{\psi}_{\mathrm{ref}}(t)$, where $\|\cdot\| := \langle\cdot|\cdot\rangle^{1/2}$ denotes the norm. The quantitative comparison, shown in Fig. 6, confirms that the quantum dynamics simulated using the exact quasidiabatic Hamiltonian is

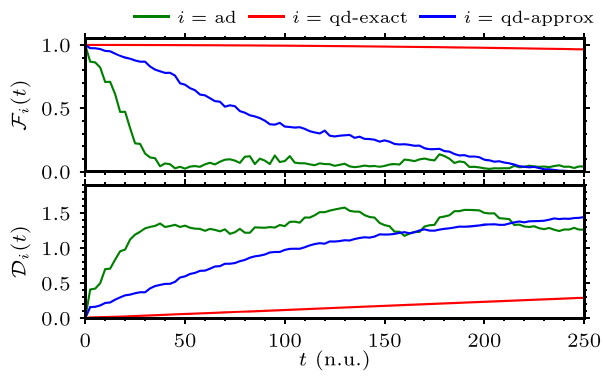

FIG. 6. Time dependence of the accuracy of the wavepackets propagated with different forms of the molecular Hamiltonian. The difference between $\tilde{\psi}_i(t)$ and the benchmark wavepacket $\tilde{\psi}_{\mathrm{ref}}(t)$ is measured either with the quantum fidelity[86] $\mathcal{F}_i(t) = |\langle\tilde{\psi}_{\mathrm{ref}}(t)|\tilde{\psi}_i(t)\rangle|^2$ (top panel) or distance $\mathcal{D}_i(t) = \|\tilde{\psi}_i(t) - \tilde{\psi}_{\mathrm{ref}}(t)\|$ (bottom panel). Fidelity and distance were computed every hundredth time step.

the most accurate: Quantum fidelity $\mathcal{F}_{\text{qd-exact}}(t)$ remains close to its maximal value of $\mathcal{F}_{\max} = 1$ until the final time. Likewise, the distance $\mathcal{D}_{\text{qd-exact}}(t_f)$ at the final time is small (although nonzero). Because $\mathcal{F}_{\text{qd-exact}}(t)$ stays close to its maximal value, the nonzero distance between $\tilde{\psi}_{\text{qd-exact}}(t)$ and $\tilde{\psi}_{\text{ref}}(t)$"] is likely to be mostly due to an overall phase difference, which does not affect the local-in-time observables, such as population or position, computed from the wavepackets [as shown in panels (b) of Figs. 3 and 4]. Even the approximate quasidiabatic Hamiltonian leads to a more accurate simulation of the quantum dynamics in the vicinity of a conical intersection than the adiabatic Hamiltonian, which has the numerically problematic singularity of $\mathbf{F}_{\text{ad}}(Q)$ at $Q = 0$.[42] The rapid initial decrease in $\mathcal{F}_{\text{ad}}(t)$ and increase in $\mathcal{D}_{\text{ad}}(t)$ show that the wavepacket dynamics simulated using $\hat{\mathbf{H}}_{\text{ad}}$ deviates quickly from the benchmark solution. The decay of fidelity and increase in the distance are much more gradual in the simulations with the approximate quasidiabatic Hamiltonian, although both rates of change are still much faster than the rates in the exact quasidiabatic simulation.

IV. CONCLUSION

We rigorously compared the suitability of different forms of the molecular Hamiltonian for simulating the nonadiabatic quantum dynamics in the vicinity of a conical intersection. This comparison was possible by taking advantage of the high-order geometric integrators and exceptional existence of the strictly diabatic Hamiltonian for the $E \otimes e$ Jahn–Teller model. The errors due to using the different forms of the molecular Hamiltonian were measured by comparing the fully converged exact reference simulation with simulations performed on a slightly sparser grid using the adiabatic, exact quasidiabatic, or approximate quasidiabatic Hamiltonian. We found that the nonadiabatic quantum dynamics simulated using the exact quasidiabatic Hamiltonian is nearly identical to the reference simulation obtained using the strictly diabatic Hamiltonian. The regularized diabatization scheme[43,46,82] was used for its simplicity, but the exact quasidiabatic Hamiltonian obtained through other schemes should lead to very similar and accurate results, as long as the quasidiabatization removes the conical intersection singularity, because Hamiltonian (8) is exact regardless of the quasidiabatization scheme. In contrast, the accuracy of the simulation with the approximate quasidiabatic Hamiltonian depends on the size of the neglected residual nonadiabatic couplings and, therefore, on the quasidiabatization scheme.[40]

To return to the question posed in the title, the approximate quasidiabatic Hamiltonian is appropriate if a quick solution of only moderate accuracy is required because the simple separable form of this Hamiltonian allows using more efficient time-propagation algorithms. The accuracy can be further improved by employing more sophisticated quasidiabatization schemes, which reduce the size of the neglected residual couplings. The adiabatic Hamiltonian, although exact, is not suitable for simulating quantum dynamics at a conical intersection because of the singularity of the nonadiabatic couplings there; large errors appeared since this singularity could not be described well on a finite grid. Although it was not the subject of this study, the adiabatic Hamiltonian is suitable for describing quantum dynamics of a high-dimensional wavepacket moving around (i.e., not exactly through) a conical intersection, especially in on-the-fly *ab initio* trajectory-based simulations, in which the adiabatic Hamiltonian is obtained directly from electronic structure calculations, because a finite number of trajectories propagated in such simulations are unlikely to pass directly through the conical intersection.[48,87–90] Yet, our results clearly show that the rarely used exact quasidiabatic Hamiltonian is the most suitable form of the molecular Hamiltonian for simulating nonadiabatic quantum dynamics directly at a conical intersection with high accuracy. Due to the inclusion of residual nonadiabatic couplings in the Hamiltonian, one may use any, even the simplest quasidiabatization scheme that removes the conical intersection singularity.

SUPPLEMENTARY MATERIAL

See the supplementary material for the geometric phase effect in the $E \otimes e$ Jahn–Teller model, preservation of the geometric properties by the employed time propagation schemes, the time and spatial discretization errors of the wavepacket and presented observables, and the nonadiabatic dynamics simulated without including the geometric phase.

ACKNOWLEDGMENTS

The authors acknowledge the financial support from the European Research Council (ERC) under the European Union's Horizon 2020 research and innovation program (Grant Agreement No. 683069—MOLEQULE) and thank Tomislav Begušić and Nikolay Golubev for useful discussions.

DATA AVAILABILITY

The data that support the findings of this study are available within the article and its supplementary material.

REFERENCES

[1] E. Teller, J. Phys. Chem. **41**, 109 (1937).
[2] T. Förster, Pure Appl. Chem. **24**, 443 (1970).
[3] G. Herzberg and H. C. Longuet-Higgins, Faraday Discuss. **35**, 77 (1963).
[4] H. E. Zimmerman, J. Am. Chem. Soc. **88**, 1566 (1966).
[5] H. Köppel, W. Domcke, and L. S. Cederbaum, Adv. Chem. Phys. **57**, 59 (1984).
[6] D. R. Yarkony, J. Chem. Phys. **92**, 2457 (1990).
[7] G. J. Atchity, S. S. Xantheas, and K. Ruedenberg, J. Chem. Phys. **95**, 1862 (1991).
[8] F. Bernardi, S. De, M. Olivucci, and M. A. Robb, J. Am. Chem. Soc. **112**, 1737 (1990).
[9] M. Klessinger and J. Michl, *Excited States and Photochemistry of Organic Molecules* (VCH Publishers, 1995).
[10] M. Baer, *Beyond Born–Oppenheimer: Electronic Nonadiabatic Coupling Terms and Conical Intersections*, 1st ed. (Wiley, 2006).
[11] W. Domcke and D. R. Yarkony, Annu. Rev. Phys. Chem. **63**, 325 (2012).
[12] H. Nakamura, *Nonadiabatic Transition: Concepts, Basic Theories and Applications*, 2nd ed. (World Scientific Publishing Company, 2012).
[13] K. Takatsuka, T. Yonehara, K. Hanasaki, and Y. Arasaki, *Chemical Theory Beyond the Born-Oppenheimer Paradigm: Nonadiabatic Electronic and Nuclear Dynamics in Chemical Reactions* (World Scientific, Singapore, 2015).
[14] M. P. Bircher, E. Liberatore, N. J. Browning, S. Brickel, C. Hofmann, A. Patoz, O. T. Unke, T. Zimmermann, M. Chergui, P. Hamm, U. Keller, M. Meuwly, H.-J. Woerner, J. Vaníček, and U. Rothlisberger, Struct. Dyn. **4**, 061510 (2017).
[15] S. Shin and H. Metiu, J. Chem. Phys. **102**, 9285 (1995).

[16]J. Albert, D. Kaiser, and V. Engel, J. Chem. Phys. **144**, 171103 (2016).
[17]A. Abedi, N. T. Maitra, and E. K. Gross, Phys. Rev. Lett. **105**, 123002 (2010).
[18]L. S. Cederbaum, J. Chem. Phys. **128**, 124101 (2008).
[19]G. A. Worth and L. S. Cederbaum, Annu. Rev. Phys. Chem. **55**, 127 (2004).
[20]L. S. Cederbaum, *Conical Intersections: Electronic Structure, Dynamics and Spectroscopy* (World Scientific, 2004), pp. 3–40.
[21]H. C. Longuet-Higgins, U. Öpik, M. H. L. Pryce, and R. Sack, Proc. R. Soc. London, Ser. A **244**, 1 (1958).
[22]C. A. Mead and D. G. Truhlar, J. Chem. Phys. **70**, 2284 (1979).
[23]M. V. Berry, Proc. R. Soc. London, Ser. A **392**, 45 (1984).
[24]C. A. Mead, Rev. Mod. Phys. **64**, 51 (1992).
[25]B. K. Kendrick, J. Chem. Phys. **112**, 5679 (2000).
[26]J. C. Juanes-Marcos and S. C. Althorpe, J. Chem. Phys. **122**, 204324 (2005).
[27]C. L. Malbon, X. Zhu, H. Guo, and D. R. Yarkony, J. Chem. Phys. **145**, 234111 (2016).
[28]C. Xie, C. L. Malbon, H. Guo, and D. R. Yarkony, Acc. Chem. Res. **52**, 501 (2019).
[29]C. Xie, D. R. Yarkony, and H. Guo, Phys. Rev. A **95**, 022104 (2017).
[30]I. G. Ryabinkin, L. Joubert-Doriol, and A. F. Izmaylov, Acc. Chem. Res. **50**, 1785 (2017).
[31]L. Joubert-Doriol, I. G. Ryabinkin, and A. F. Izmaylov, J. Chem. Phys. **139**, 234103 (2013).
[32]J. Schön and H. Köppel, J. Chem. Phys. **103**, 9292 (1995).
[33]C. Leforestier, R. H. Bisseling, C. Cerjan, M. D. Feit, R. Friesner, A. Guldberg, A. Hammerich, G. Jolicard, W. Karrlein, H.-D. Meyer, N. Lipkin, O. Roncero, and R. Kosloff, J. Comput. Phys. **94**, 59 (1991).
[34]H. Tal-Ezer and R. Kosloff, J. Chem. Phys. **81**, 3967 (1984).
[35]T. J. Park and J. C. Light, J. Chem. Phys. **85**, 5870 (1986).
[36]E. Hairer, C. Lubich, and G. Wanner, *Geometric Numerical Integration: Structure-Preserving Algorithms for Ordinary Differential Equations* (Springer Berlin Heidelberg, New York, 2006).
[37]M. D. Feit, J. A. Fleck, Jr., and A. Steiger, J. Comput. Phys. **47**, 412 (1982).
[38]C. Lubich, *From Quantum to Classical Molecular Dynamics: Reduced Models and Numerical Analysis*, 12th ed. (European Mathematical Society, Zürich, 2008).
[39]D. J. Tannor, *Introduction to Quantum Mechanics: A Time-Dependent Perspective* (University Science Books, Sausalito, 2007).
[40]S. Choi and J. Vaníček, arXiv preprint arXiv:2011.09191.
[41]C. A. Mead and D. G. Truhlar, J. Chem. Phys. **77**, 6090 (1982).
[42]T. Pacher, C. A. Mead, L. S. Cederbaum, and H. Köppel, J. Chem. Phys. **91**, 7057 (1989).
[43]H. Köppel, J. Gronki, and S. Mahapatra, J. Chem. Phys. **115**, 2377 (2001).
[44]T. Pacher, L. S. Cederbaum, and H. Köppel, J. Chem. Phys. **89**, 7367 (1988).
[45]F. X. Gadéa and M. Pélissier, J. Chem. Phys. **93**, 545 (1990).
[46]A. Thiel and H. Köppel, J. Chem. Phys. **110**, 9371 (1999).
[47]A. Viel, R. P. Krawczyk, U. Manthe, and W. Domcke, J. Chem. Phys. **120**, 11000 (2004).
[48]M. Ben-Nun, J. Quenneville, and T. J. Martínez, J. Phys. Chem. A **104**, 5161 (2000).
[49]L. M. Ibele and B. F. E. Curchod, Phys. Chem. Chem. Phys. **22**, 15183 (2020).
[50]A. Mandal, S. S. Yamijala, and P. Huo, J. Chem. Theory Comput. **14**, 1828 (2018).
[51]W. Zhou, A. Mandal, and P. Huo, J. Phys. Chem. Lett. **10**, 7062 (2019).
[52]H. Guo and D. R. Yarkony, Phys. Chem. Chem. Phys. **18**, 26335 (2016).
[53]C. Xie, J. Ma, X. Zhu, D. R. Yarkony, D. Xie, and H. Guo, J. Am. Chem. Soc. **138**, 7828 (2016).
[54]I. B. Bersuker and V. Z. Polinger, *Vibronic Interactions in Molecules and Crystals* (Springer Science + Business Media, 2012), Vol. 49.
[55]I. B. Bersuker, Chem. Rev. **101**, 1067 (2001).
[56]B. Leimkuhler and S. Reich, *Simulating Hamiltonian Dynamics* (Cambridge University Press, 2004).
[57]M. Suzuki, Phys. Lett. A **146**, 319 (1990).
[58]H. Yoshida, Phys. Lett. A **150**, 262 (1990).
[59]W. Kahan and R.-C. Li, Math. Comput. **66**, 1089 (1997).
[60]S. Choi and J. Vaníček, J. Chem. Phys. **150**, 204112 (2019).
[61]J. Roulet, S. Choi, and J. Vaníček, J. Chem. Phys. **150**, 204113 (2019).
[62]M. Born and K. Huang, *Dynamical Theory of Crystal Lattices* (Oxford University Press, London, 1954).
[63]C. J. Ballhausen and A. E. Hansen, Annu. Rev. Phys. Chem. **23**, 15 (1972).
[64]D. R. Yarkony, Rev. Mod. Phys. **68**, 985 (1996).
[65]H. Köppel, *Conical Intersections: Electronic Structure, Dynamics and Spectroscopy* (World Scientific, 2004), pp. 175–204.
[66]D. R. Yarkony, *Conical Intersections: Electronic Structure, Dynamics and Spectroscopy* (World Scientific, 2004), pp. 41–127.
[67]T. Pacher, H. Köppel, and L. S. Cederbaum, J. Chem. Phys. **95**, 6668 (1991).
[68]S. P. Neville, I. Seidu, and M. S. Schuurman, J. Chem. Phys. **152**, 114110 (2020).
[69]W. Domcke and C. Woywod, Chem. Phys. Lett. **216**, 362 (1993).
[70]M. Baer, Chem. Phys. Lett. **35**, 112 (1975).
[71]A. Das, D. Mukhopadhyay, S. Adhikari, and M. Baer, Chem. Phys. Lett. **517**, 92 (2011).
[72]G. W. Richings and G. A. Worth, J. Phys. Chem. A **119**, 12457 (2015).
[73]R. G. Sadygov and D. R. Yarkony, J. Chem. Phys. **109**, 20 (1998).
[74]B. D. Esry and H. R. Sadeghpour, Phys. Rev. A **68**, 042706 (2003).
[75]R. S. Mulliken, J. Am. Chem. Soc. **74**, 811 (1952).
[76]N. S. Hush, Prog. Inorg. Chem. **8**, 391 (1967).
[77]R. J. Cave and M. D. Newton, J. Chem. Phys. **106**, 9213 (1997).
[78]H. J. Werner and W. Meyer, J. Chem. Phys. **74**, 5802 (1981).
[79]D. R. Yarkony, J. Phys. Chem. A **102**, 8073 (1998).
[80]G. Hirsch, R. J. Buenker, and C. Petrongolo, Mol. Phys. **70**, 835 (1990).
[81]M. Perić, S. D. Peyerimhoff, and R. J. Buenker, Mol. Phys. **71**, 693 (1990).
[82]H. Köppel and B. Schubert, Mol. Phys. **104**, 1069 (2006).
[83]H. Köppel, Faraday Discuss. **127**, 35 (2004).
[84]J. Crank and P. Nicolson, Math. Proc. Cambridge Philos. Soc. **43**, 50 (1947).
[85]E. A. McCullough, Jr. and R. E. Wyatt, J. Chem. Phys. **54**, 3578 (1971).
[86]A. Peres, Phys. Rev. A **30**, 1610 (1984).
[87]B. F. E. Curchod and T. J. Martínez, Chem. Rev. **118**, 3305 (2018).
[88]B. Lasorne, M. J. Bearpark, M. A. Robb, and G. A. Worth, Chem. Phys. Lett. **432**, 604 (2006).
[89]G. A. Worth, M. A. Robb, and I. Burghardt, Faraday Discuss. **127**, 307 (2004).
[90]K. Saita and D. V. Shalashilin, J. Chem. Phys. **137**, 22A506 (2012).